# Importance and Reduction of the Sidewall-Induced Band-Broadening Effect in Pressure-Driven Microfabricated Columns

**ARTICLE** *in* ANALYTICAL CHEMISTRY · SEPTEMBER 2004

Impact Factor: 5.64 · DOI: 10.1021/ac049930h · Source: PubMed



**5 AUTHORS**, INCLUDING:

Nico Vervoort
Janssen Pharmaceutica
**25** PUBLICATIONS **745** CITATIONS
SEE PROFILE

Gert Desmet
Vrije Universiteit Brussel
**254** PUBLICATIONS **3,745** CITATIONS
SEE PROFILE

*Anal. Chem.* **2004,** *76,* 4501−4507

# Importance and Reduction of the Sidewall-Induced Band-Broadening Effect in Pressure-Driven Microfabricated Columns

Nico Vervoort,* Jeroen Billen, Piotr Gzil, Gino V. Baron, and Gert Desmet

*Vrije Universiteit Brussel, Department of Chemical Engineering, Pleinlaan 2, 1050 Brussels, Belgium*

**The influence of the detailed design of the sidewall region upon the over-all band-broadening in microfabricated packed-bed or collocated monolithic support structure (COMOSS) columns has been investigated using computational fluid dynamics (CFD) simulation techniques. It is shown that, under unretained solute conditions, very small structural variations of the order of only 5% of the particle diameter can give rise to a 4-fold increase of the band-broadening. A comprehensive study has been made to quantify this effect as a function of the fluid velocity, the particle diameter, the channel widths, and of course, the sidewall region design. Because the sidewall effect can be fully attributed to a mismatch between the flow rates in the column center and in the sidewall region, it is fortunately also quite straightforward to avoid it. A very simple design, yielding band-broadening values identical to that of a hypothetical sidewall-less column for all possible values of the flow velocity, the particle diameter, or the channel width is proposed.**

The past decade has witnessed the advent of the so-called lab-on-a-chip (LoC) field. The highly miniaturized systems which are currently under development in this field promise to offer the analysis speed and efficiency needed to fulfill the need for high-throughput analytical screening in life science research, clinical diagnosis, drug discovery, biotechnology, and environmental monitoring. In the past years, several modes of operation, such as capillary electrophoresis (CE), micellar electrokinetic chromatography (MEKC), and packed bed liquid chromatography (LC) and open tubular LC, have already been successfully applied to separate charged and neutral species in silicon or glass-etched microfluidic channels.[1−5] The majority of the successful LoC applications (such as CE), however, is based on the use of open channels, typically ∼10 $\mu$m deep and ∼100 $\mu$m wide. The major problem with the use of open tubular channels for applications such as LC or affinity assays is their limited loading capacity. To widen the range of LoC applications, there is, hence, a clear need to increase the surface capacity of the microchannels.[6] One straightforward approach to achieve this is to pack the channels with small porous particles or deposit a high surface monolithic material in the microchannels. Packing these tiny channels with porous particles, however, turns out to be very tedious,[7] and the deposition of a polymer or silica monolithic material inside the channel is not straightforward, either. Another radically different approach to enhance the surface area in microchannels was proposed by Regnier and his group.[8−11] Their approach consisted of using microlithography techniques, adopted from microelectronics, to micromachine 2D packed-bed channels containing so-called collocated monolithic support structures (COMOSS) onto the surface of a silicon wafer. This approach offers several benefits: there is no need to pack the channel with particles anymore; it allows for the creation of multiple columns onto a single wafer; and with the large degree of freedom with which the shape and positioning of the COMOSS-particles can be machined, an additional optimization variable is introduced. Since these micromachined packings offer the possibility to combine the small dimensions needed to overcome the mass transfer limitation with a high surface area, they seem to be ideal candidates to replace the classical packed-bed column in analytical applications requiring fast and efficient separation of compounds.

The present study has been set up to investigate the effect of the sidewall region in such columns upon the total band-broadening under pressure-driven conditions. We were prompted to this problem by the recent work of Dutta and Leigthon,[12] showing that, under pressure-driven conditions, the presence of sidewalls increases the band-broadening in open tubular etched microchannels by a factor of ∼8, as compared to an infinite channel without sidewalls. Dutta & Leighton have also shown that the solute dispersion in isotropically etched channels can be reduced by modifying the channel geometry near the wall (the double-etch profile). The reader should note that the problem under investigation is exclusively related to pressure-driven flows, since electrokinetically driven flows are supposed to be insensitive to local differences in flow resistance.

* Corresponding author. Phone: (+)32-2-629-36-17. Fax: (+)32-2-629-32-48. E-mail: nvervoor@vub.ac.be.

(1) Woolley, A. T.; Lao, K.; Glazer, N.; Mathies, R. A. *Anal. Chem.* **1998**, *70*, 684−688.
(2) Manz, A.; Miyahara, Y.; Miura, J.; Watanabe, Y.; Miyagi, H.; Sato, K. *Sens. Actuators, A* **1990**, *B1*, 249−255.
(3) Verpoorte, E. *Electrophoresis* **2002**, *23*, 677−712.
(4) Peterson, D. S.; Rohr, T.; Svec, F.; Fréchet, J. M. J. *Anal. Chem.* **2003**, *75*, 5328−5335.
(5) Stachowiak, T. B.; Rohr, T.; Hilder, E. F.; Peterson, D. S.; Yi, M.; Svec, F.; Fréchet, J. M. J. *Electrophoresis* **2003**, *24*, 3689−3693.
(6) Buranda, T.; Huang, J. M.; Perez-Luna, V. H.; Schreyer, B.; Sklar, L. A.; Lopez, G. P. *Anal.Chem.* **2002**, *74*, 1149−1156.
(7) Ocvirk, G.; Verpoorte, E.; Manz, A.; Grasserbauer, M.; Widmer, H. M. *Anal. Methods Instrum.* **1995**, *2*, 74−82.
(8) He, B.; Regnier, F. J. *Pharm. Biomed. Anal.* **1998**, *17*, 925−932.
(9) Regnier, F. E. *J. High Resolut. Chromatogr.* **2000**, *23*, 19−26.
(10) Slentz, B. E.; Penner, N. A.; Regnier, F. J. *Sep. Sci.* **2002**, *25*, 1011−1018.
(11) Slentz, B. E.; Penner, N. A.; Lugowska, E.; Regnier, F. *Electrophoresis* **2001**, *22*, 3736−3743.
(12) Dutta, D.; Leighton, D. T. *Anal.Chem.* **2001**, *73*, 504−513.

10.1021/ac049930h CCC: $27.50 
Published on Web 07/08/2004

Considering now packed or microstructured columns, in which the sidewall area only makes up a very small fraction of the total packing surface area, it is difficult to contemplate in advance whether the sidewall effect will be as prominent as in the open tubular case.

To answer this question, the dispersion of a tracer species plug moving through microstructured packing was studied by means of computational fluid dynamics (CFD). This technique uses an iterative numerical solution method to solve the discretized species and momentum conservation equations, yielding a detailed knowledge of the velocity, pressure, and species distribution in the system.[13−16] CFD simulation techniques prove to be very helpful for the design of novel flow systems. They eliminate the need to fabricate large numbers of different columns, which is both time-consuming and costly. Furthermore, since the dimensions of the geometry are exactly known, the obtained data are not influenced by fabrication defects, something which seems to be difficult to avoid in practice.[10] The fact that no complicated injection and detection setup is needed is another advantage.

In the present study, we focused on the case of a cylindrical pillar bed with an external porosity of $\epsilon = 0.4$, because this corresponds most closely to the packed bed of spheres traditionally employed in analytical separations. We believe, however, that the conclusions of the present study will also hold (at least qualitatively) for other bed porosities and particle shapes. Because we wanted to focus on the effect of the flow distribution itself, we excluded any solute retention effect by treating the cylindrical pillars as nonporous, fully inert flow obstacles.

## CONSIDERED STRUCTURE AND CFD SOLUTION METHOD

The considered packing design consists of an array of cylindrical pillars with diameter $d_p$ (Figure 1). The pillars are arranged in an equilateral triangular conformation, i.e., $z_2 = \sqrt{3}z_1$ in Figure 1. For the considered bed porosity of $\epsilon = 0.4$, it can easily be verified that $z_1 = 1.23d_p$ and $z_2 = 2.13d_p$. As shown in Figure 1, three general cases have been considered: the infinite channel case, obtained by considering a hypothetical structure with symmetry plane boundaries (Figure 1a); the embedded cylinder wall case (Figure 1b); and the straight wall case, corresponding to a channel layout with perfectly straight running sidewalls and with a fixed spacing $\Delta w$ between the exterior cylinder row and the sidewalls (Figure 1c). All considered columns had a length of 300 $\mu$m, because this value was found to be sufficiently large to obtain the long-term solution wherein the plate height has converged to its limiting value (cf. the discussion of Figure 5). To obtain generally applicable results, the channel width $w$ and the wall spacing $\Delta w$ were reduced on the basis of the particle diameter $d_p$, yielding the following dimensionless parameters:

$$\omega = \frac{w}{d_p} \quad \text{and} \quad \Delta\omega = \frac{\Delta w}{d_p} \tag{1}$$

Simulations were carried out for various $\Delta\omega$ and $\omega$ values and at different velocities. Two values of $d_p$ were considered, 3 and 5 $\mu$m. To investigate the influence of the column width, $w$ was varied between 10 and 100 $\mu$m.

The CFD simulations were carried out with a commercially available CFD package, FLUENT (v.6.1). The software was

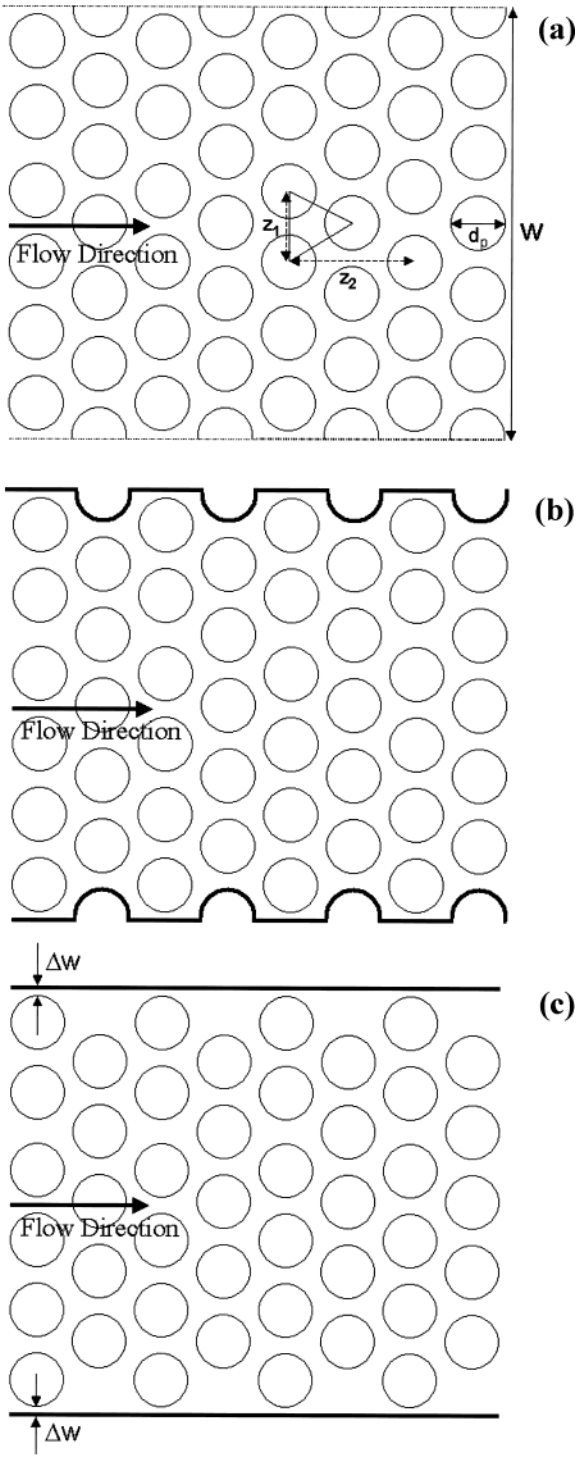


Figure 1. Schematic top view of the different considered channel geometries: (a) a hypothetical, infinitely wide channel obtained by treating the dashed channel boundaries as symmetry planes; (b) a channel with halved cylinder particles embedded into its sidewalls; and (c) a channel with perfectly flat sidewalls, with a spacing $\Delta\omega$ between the walls and the first row of cylinders. Also represented are the main geometrical parameters $d_p$, $w$, $z_1$, and $z_2$.


(13) Wu, Y. X.; Ching, C. B. *Chromatographia* **2002**, *56*, 679−686.
(14) Vervoort, N.; Gzil, P.; Baron, G. V.; Desmet, G. *Anal. Chem.* **2003**, *75*, 843−850.
(15) Gzil, P.; Baron, G. V.; Desmet, G. *J. Chromatogr., A* **2003**, *991*, 169−188.
(16) Gzil, P.; Vervoort, N.; Baron, G. V.; Desmet, G. *Anal. Chem.* **2003**, *75*, 6244−6250.

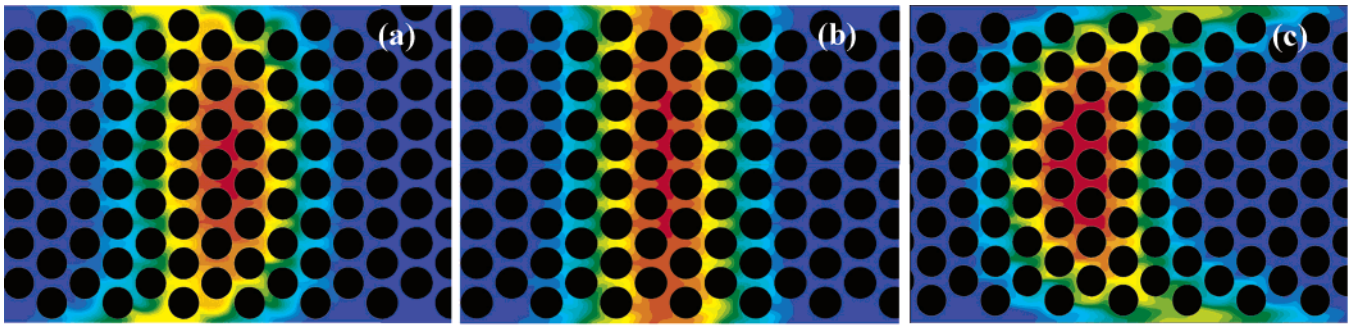


Figure 2. Contour plots of a species plug 0.1 s after its injection for three different $\Delta\omega$ values: (a) 0.115, (b) 0.150, and (c) 0.200. Other conditions: $\nu = 23$, $d_p = 5$ $\mu$m, $w = 62.5$ $\mu$m. The color scale varies from blue (smallest concentration) to red (largest concentration).

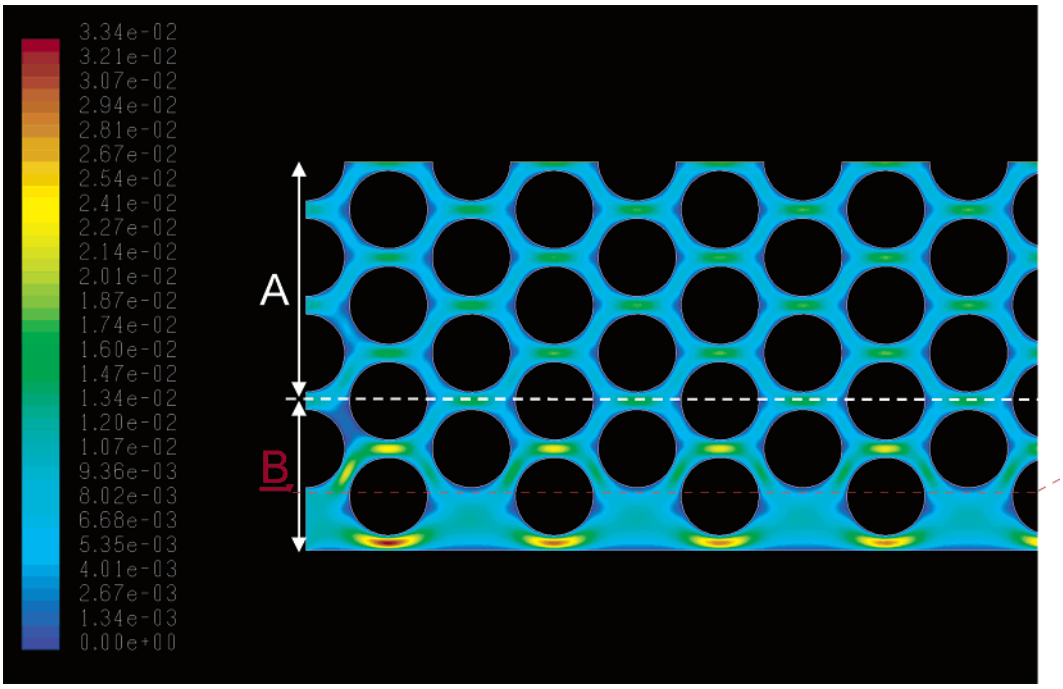


Figure 3. Velocity contour plot for the channel layout considered in Figure 2c, also showing the two regions (A and B) used to calculate the average center velocity ($u_{center}$) and the average wall velocity ($u_{wall}$), respectively. The color intensity scale is in meters per second. To yield a maximally zoomed view, only the bottom half of the column is represented.

installed on a PC with an Intel Pentium IV processor running at 2800 MHz and equipped with 1 Gb RAM. The grids were generated with GAMBIT (v.2.0.4) software, run on the same hardware configuration. The boundary conditions on the sidewalls were set at either "symmetry" (such that the system behaves as an infinitely wide medium) or "wall" (no-slip and no-net flux condition), depending on the case. The boundary conditions for the cylinder surfaces were always put at "walls". The inlet was treated as a velocity inlet with uniform velocity distribution. The outlet was treated as a pressure outlet with governing atmospheric pressure. All cases were solved using a second-order discretization scheme, and the residual drop was at least 6 orders of magnitude. Water, with a density of 1000 kg/m$^3$ and a viscosity of $1 \times 10^{-3}$ kg/(m·s), was chosen as the working fluid. The tracer (dye) had the same properties as water, with a molecular diffusion coefficient put at $D_m = 10^{-9}$ m$^2$/s. After the solution for the velocity field was converged, the flow field calculation was switched off, a 20-$\mu$m-long virtually injected plug of tracer dye was injected at the beginning of the column, and the governing equations describing the unsteady-state species transport were solved. The average mass fraction of the passing dye plug was recorded as a function of time at several subsequent monitor planes. These were regularly positioned along the channel axis, starting from $x = 0$ and with an interval equal to $z_2$. The response curves were subsequently used to calculate retention times and theoretical plate height values by numerically calculating the zeroth-, first-, and second-order moment of the obtained break-through curves using

$$t_{R,i} = \frac{\int_0^{+\infty} C_i t \, dt}{\int_0^{+\infty} C_i \, dt} \tag{2}$$

$$\sigma_{t,i}^2 = \frac{\int_0^{+\infty} C_i t^2 \, dt}{\int_0^{+\infty} C_i \, dt} - t_{R,i}^2 \tag{3}$$

wherein $t_{R,i}$ is the retention time of the plug when passing monitor plane i, and $C_i$ is the concentration of dye at plane i. From eqs 2

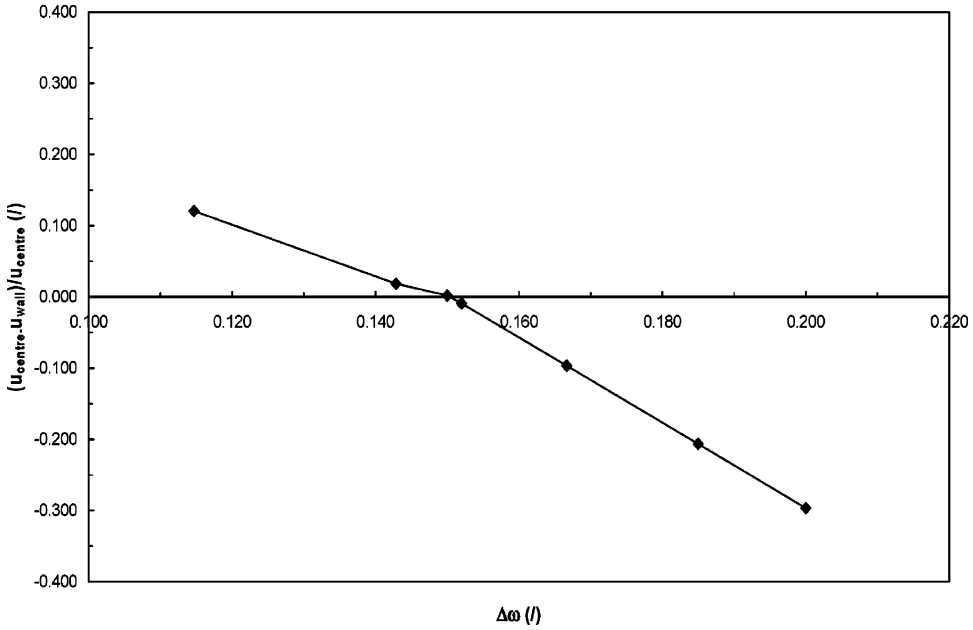


Figure 4. Variation of the $(u_{center} - u_{wall})/u_{center}$ ratio as a function of the wall spacing $\Delta\omega$, showing that for $\Delta\omega = 0.150$, the average velocity in both regions is equal. In the adopted dimensionless representation, the data points for $d_p = 3$ and 5 $\mu$m exactly coincided and could not be distinguished from each other.

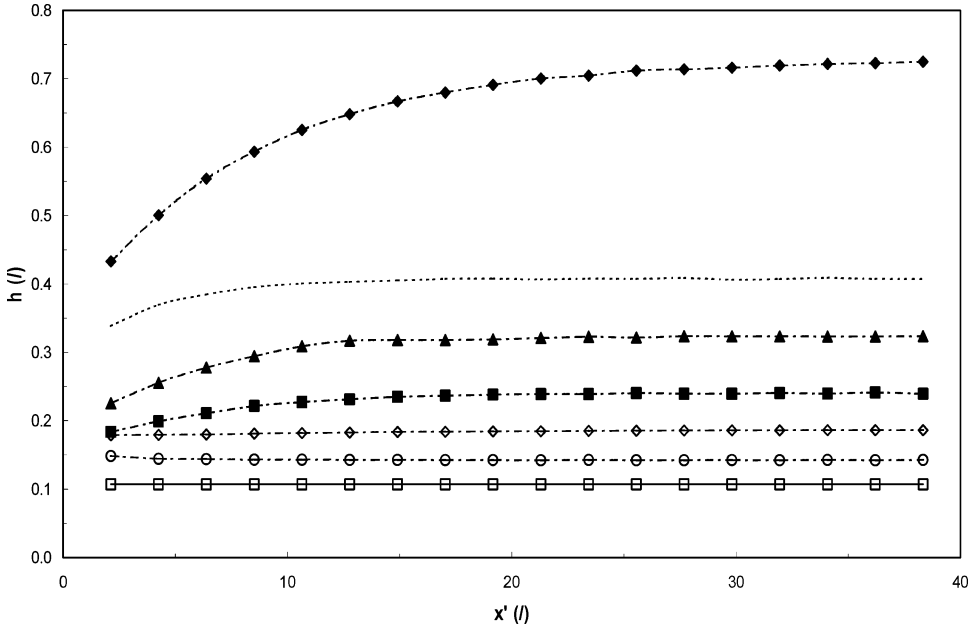


Figure 5. Reduced plate height values as function of the dimensionless position $x'$ of the monitor planes: —, infinite channel case; - - - - -, embedded cylinder case. Straight wall cases: ◆, $\Delta\omega = 0.200$; ▲, $\Delta\omega = 0.115$; ■, $\Delta\omega = 0.125$; ◇, $\Delta\omega = 0.167$; △, $\Delta\omega = 0.143$; □, $\Delta\omega = 0.150$. Other conditions: $d_p = 5$ $\mu$m and $\nu = 16$.

and 3, the theoretical plate height values can be directly obtained using

$$H = \frac{\sigma_{t,j}^2 - \sigma_{t,i}^2}{(t_{R,j} - t_{R,i})^2} L_{ij} \qquad (4)$$

The obtained values were subsequently made dimensionless using the cylinder diameter ($h = H/d_p$) as the reduction basis.

## RESULTS AND DISCUSSION

**Influence of the Sidewall Design.** The most important variable in the presently considered problem obviously is the sidewall design itself. Figure 2 qualitatively compares the influence of the spacing distance on the species band profile in the straight sidewall case of Figure 1c. It can clearly be noted that when going from $\Delta\omega = 0.115$ (Figure 2a) to $\Delta\omega = 0.200$ (Figure 2c), the species band profile switches from a situation wherein the tracer species near the wall lags behind the center of the plug to a situation wherein the tracer species near the wall runs ahead of the central channel region. This tailing/fronting effect obviously stems from the differences in mean velocity between the central and sidewall regions of the channel. This is further investigated in Figure 3, which shows the local velocity contour plot of the case shown in Figure 2c. It can clearly be noted that due to the

slightly larger flow-through pore width, the velocity near the sidewalls is larger than in the central region of the column. For the geometry considered in Figure 2a (data not represented here), the opposite situation was noted. To quantify the velocity difference between the sidewall and the column bulk region, the column has been more or less arbitrarily divided into two parts (see Figure 3), a center region (A) and a wall region (B). In the central region, the velocity is identical in each flow-through pore, whereas in the wall region, the velocity is clearly different. Calculating the average velocity in each region and plotting the resulting $(u_{center} - u_{wall})/u_{center}$ ratio as a function of the different considered $\Delta\omega$ values (Figure 4), this ratio clearly continuously decreases with increasing wall spacing $\Delta\omega$, going from a value of ~0.11 for $\Delta\omega = 0.115$ to a value of ~0.3 for $\Delta\omega = 0.20$ and crossing the $(u_{center} - u_{wall})/u_{center} = 0$ line at $\Delta\omega = 0.150$. In full agreement with our physical expectations, it was verified that this critical $\Delta\omega = 0.150$ value is independent of the position of the plane separating the center and the wall region (cf. the dashed line in Figure 3). The position of this plane only influences the slope of the $(u_{center} - u_{wall})/u_{center}$ lines, but not the position of the $(u_{center} - u_{wall})/u_{center} = 0$ crossing point.

Because the physical interpretation of the above determined $\Delta\omega = 0.150$ rule is that it corresponds to a sidewall design for which the wall spacing is exactly large enough for the average velocity in the sidewall region to exactly match that of the center region, this should, of course, be reflected in the profile of the species bands. As can be noted in Figure 2b, the $\Delta\omega = 0.150$ condition indeed leads to a situation wherein the species band moves through the column in a quasiperfect straight line. From the fact that the data for $d_p = 3$ and 5 $\mu$m in Figure 4 perfectly coincide, it can be concluded that the $\Delta\omega = 0.150$ rule is independent of the diameter of the pillars, as could be anticipated on pure physical grounds.

To quantify the magnitude of the sidewall effect, the passage of the virtually injected species bands has been monitored as a function of the time on the successively positioned monitor planes. Figure 5 gives an overview of the plate height values obtained for a number of different sidewall geometries ($d_p = 5$ $\mu$m in all cases), by applying eq 4 between each pair of successive monitor lines. The data for $d_p = 3$ $\mu$m are not represented, because they perfectly coincided with the $d_p = 5$ $\mu$m data in the adopted dimensionless coordinate representation. The gradual increase of $h$ with $x'$ (referred to as the transient regime), which is observed in most of the cases, of course stems from the fact that the tracer species need a certain time to equilibrate between the center region and the wall region of the channel before a steady regime is obtained. The existence of such a transient regime is also noted in the open tubular channel studies of Dutta and Leighton.

Taking now a closer look on the obtained $h$ values, it can immediately be noted that, as physically expected, the (hypothetical) infinite column case (cf. Figure 1a) yields the smallest band-broadening ($h = 0.104$) and provides an excellent reference basis for the other considered sidewall designs. As can be noted, the difference with the embedded cylinder wall geometry (cf. Figure 1b) is quite large (roughly a factor of 4). Because the embedded cylinder case is one of the first options coming to one's mind when designing the sidewall region of a microfabricated channel, this large difference points at the large attention one should pay to the layout of the sidewall region when designing a pressure-driven microfluidics application, as has already been noted by Dutta and Leighton for the open-channel case.

Looking now at the results for the different considered straight wall designs, the long time limit plate height values obviously strongly depend on the value of $\Delta\omega$ . Because $\Delta\omega$ has only been varied from 0.115 to 0.200 (i.e., corresponding only to a variation of the cylinder-to-wall spacing of 8.5% of the cylinder diameter), the large difference between the different $\Delta\omega$ curves reemphasizes the above statement on the importance of a careful sidewall design. Because most straight sidewall cases lie below the embedded cylinder case, it should be obvious that the straight wall case design will in most cases already lead to a significant reduction of the band-broadening with respect to the embedded cylinder wall case. Even more, there exists a critical case ($\Delta\omega = 0.150$, square open symbols in Figure 5) in which the straight wall design allows complete elimination of the sidewall effect, allowing obtaining of the small low plate heights of the hypothetical infinitely wide column. An important remark here is that we only consider a theoretical exercise, whereas it may turn out to be very difficult to achieve the desired etching accuracy. Obviously, when the wall spacing becomes too large (as for the $\Delta\omega = 0.200$ case), the straight sidewall design can yield a dramatically large band-broadening.

**Influence of the Velocity.** Whereas Figure 5 only relates to the case of a single mean velocity, a wide range of other velocities, ranging from $\nu = 3$ to $\nu = 70$, and covering both the B-term-dominated range and the C-term-dominated range of the van Deemter curve, has been considered to investigate the general applicability of the $\Delta\omega = 0.150$ rule. Figure 6 summarizes some of these data and shows that the minimal plate height ($h_{min}$) is, indeed, always reached for $\Delta\omega = 0.150$, independently of the imposed mean velocity. For all represented velocities, both the $\Delta\omega < 0.150$ and $\Delta\omega > 0.150$ cases lead to a situation wherein $h$ differs significantly from $h_{min}$. This finding points at the fact that the sidewall effect is the result of an absolute difference in velocity and that its influence is independent of the sign of this difference. This is, in fact, in agreement with an analytical calculation made in ref 17, in which a long time limit value for $h$ for the case of two parallel flows with a different velocity $u_1$ and $u_2$ is established, yielding an expression which was linearly proportional to the absolute value of the velocity difference $|u_1 - u_2|$. The lack of symmetry between the $\Delta\omega < 0.150$ and $\Delta\omega > 0.150$ branches of the different $u$ curves can be brought back to the fact that the relation between $\Delta\omega$ and the velocity difference between the central and sidewall region is not linear either and displays a much steeper relation for $\Delta\omega > 0.150$ than for $\Delta\omega < 0.150$ (see Figure 4).

The fact that the $h$ values for the smallest considered velocity ($\nu = 3$, upper curve in Figure 6) only depend very weekly on $\Delta\omega$ is due to the fact that this velocity already lies relatively deep in the *B*-term-dominated range of the van Deemter curve, where the influence of convective effects is of small importance. The fact that the $h$ values relate to a velocity deep in the B-term range also explains why they are relatively large, as compared to most of the other values obtained for the larger velocities.

(17) Berdichevsky, A. L.; Neue, U. D. *J. Chromatogr., A* **1990**, *535*, 189−198.

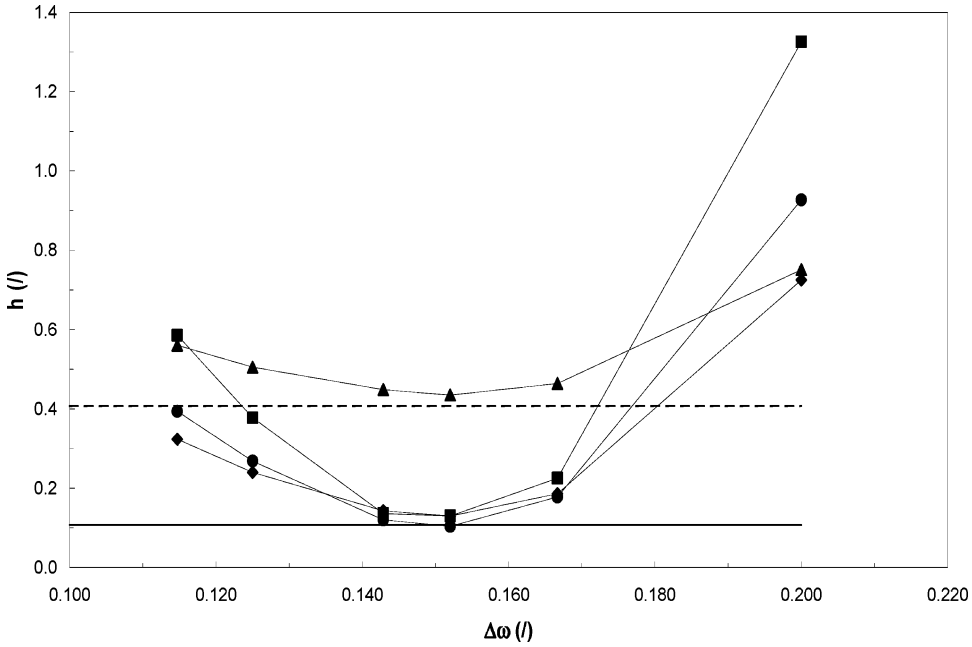


Figure 6. Reduced plate height versus $\Delta\omega$ for different velocities. ▲, $\nu = 2.3$; ◆, $\nu = 11.5$; ●, $\nu = 23$; and ■, $\nu = 46$. Other conditions: $d_p = 5\ \mu$m, $w = 62.5\ \mu$m, $D_m = 10^{-9}$ m$^2$/s.

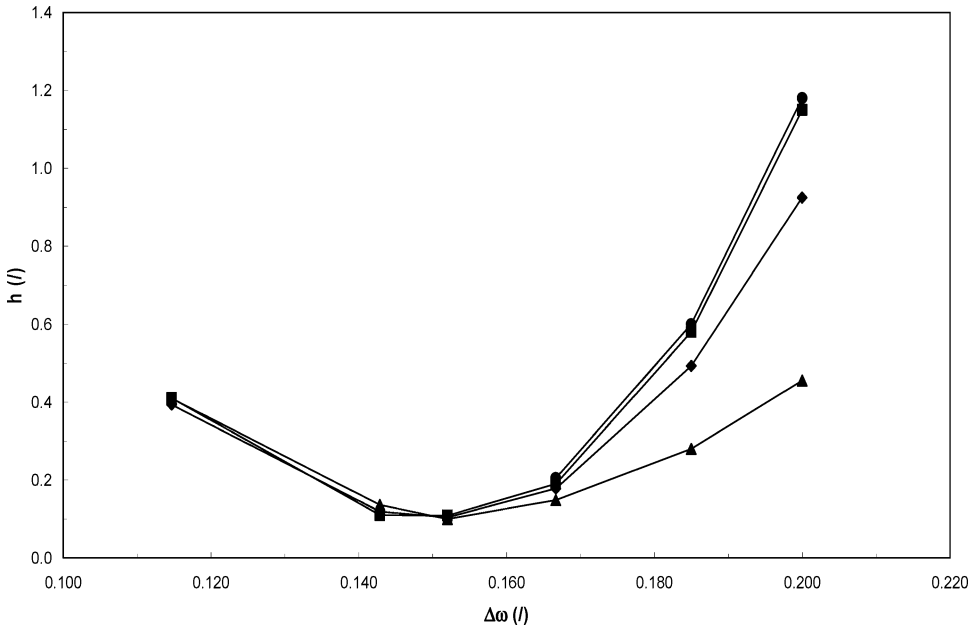


Figure 7. Reduced plate height vs $\Delta\omega$ for different dimensionless column width values: ▲, $\omega = 2.5$; ◆, $\omega = 6.25$; ■, $\omega = 10$; ●, $\omega = 20$. Other conditions: $\nu = 23$, $d_p = 5\ \mu$m, $D_m = 10^{-9}$ m$^2$/s.

**Influence of Column Width.** To further validate the general validity of the $\Delta\omega = 0.150$ design rule, the influence of the column width has been investigated, as well. Four different aspect ratios ($\omega = 2.5$, 6.25, 10, and 20) have been considered. The resulting long time-limit values are represented in Figure 7, clearly showing that the $\Delta\omega = 0.150$ rule also holds independently of the channel width. This, in fact, should not come as a surprise, since the $\Delta\omega = 0.150$ rule eliminates the sidewall problem at its root: by making the flow-through pore space in the sidewall region sufficiently large to establish equal mean velocities throughout the entire column, the sidewall tailing/fronting problem is solved in a fundamental way, independently of the mean velocity or the channel width. Looking more closely at the represented data, it can be noted that the magnitude of the sidewall effect increases with increasing channel width, but that from a given aspect ratio on, the influence of the channel width reaches a limiting value. The latter can be assessed from the fact that the difference between the $\omega = 10$ and the $\omega = 20$ lines is much smaller than the difference between the $\omega = 2.5$ and the $\omega = 6.25$ lines. Both findings are in full agreement with earlier calculations and arguments on the sidewall effect in open tubular channels with a flat rectangular cross section.[12,18–19] Again, the data for the $d_p = 3$-$\mu$m pillars are not represented, because they coincided perfectly with the $d_p = 5\ \mu$m data.

(18) Desmet, G.; Baron, G. V. *J. Chromatogr., A* **2002**, *946*, 51–58.
(19) Golay M. J. E. *J. Chromatogr., A* **1981**, *216*, 1–8.

## CONCLUSIONS

Using a series of CFD calculations, it has been shown that, although the sidewall area only makes up a negligible fraction of the total packing surface area, the sidewall region can lead to a strong increase of the band-broadening in pressure-driven 2D etched COMOSS columns (easily a factor of 2−4 in the $u \gg u_{opt}$ range). One of the obvious sidewall designs, that is, with an embedded row of half cylinders near the wall, leads to an increase in the band-broadening by a factor of 4 near the optimal velocity. The presently described sidewall effect is similar to the sidewall effect in open flat-rectangular channels described by Dutta and Leigthon. Similar to the open tubular channel case, the effect does not vanish when the channel width is increased. Also similar to the open tubular channel case, the effect can, however, be completely eliminated (at least in theory) by exactly matching the mean flow rate in the sidewall region to the mean flow rate in the central region of the channel. Whereas in the open tubular channel case, the matching of the flow rates requires a complex two step etching process, the flow rates in the COMOSS case can be simply matched by delimiting the channel region with a straight wall, put at exactly 0.150 times $d_p$ ($\Delta\omega = 0.150$) from the outer cylinder line. This $\Delta\omega = 0.150$ rule remains valid over the entire range of possible flow velocities, channel widths, and cylinder diameters. For other geometries and pillar arrangements, it can easily be inferred that the side wall effect can be eliminated in a similar manner, but presumably with a slightly different value for $\Delta\omega_{opt}$.

The presently observed strong dependency of the overall band-broadening on small variations in the sidewall design shows that a proper design of the sidewall region of pressure-driven packed microchannels is of vital importance. On the other hand, this strong influence also points to the fact that the smallest etching error could already lead to a large deviation from the theoretically expected behavior.

## ACKNOWLEDGMENT

The authors greatly acknowledge a research grant (FWO KNO 81/00) of the Fund for Scientific Research−Flanders (Belgium). P.G. is supported through a specialization grant from the Instituut voor Wetenschap en Technologie (IWT) of the Flanders Region (Grant No. SB/11419).

## NOTATION

| | |
|---|---|
| $C_i$ | concentration of dye at monitor plane i |
| $d_p$ | cylinder diameter |
| $D_m$ | molecular diffusion coefficient ($10^{-9}$ m$^2$/s) |
| $H$ | plate height |
| $h$ | reduced plate height |
| $L_{ij}$ | distance between two consecutive monitor planes |
| $t$ | time |
| $t_R$ | retention time |
| $u$ | mobile phase velocity |
| $u_{center}$ | average fluid velocity in zone A of Figure 3 |
| $u_{wall}$ | average fluid velocity in zone B of Figure 3 |
| $\Delta w$ | distance between cylinder and wall as depicted in Figure 1 |
| $w$ | channel width |
| $x'$ | channel distance made dimensionless on the basis of the particle diameter |
| $z_1$ | distance between two cylinders in the radial direction as depicted in Figure 1 |
| $z_2$ | distance between two cylinders in the axial direction as depicted in Figure 1 |

Greek Symbols

| | |
|---|---|
| $\Delta\omega$ | relative distance between the cylinder and wall as defined in eq 1 |
| $\omega$ | channel aspect ratio as defined in eq 1 |
| $\sigma$ | standard deviation |
| $\nu$ | reduced velocity, defined as $\nu = d_p u / D_m$ |

Received for review January 12, 2004. Accepted May 27, 2004.

AC049930H